

Paleoceanography and Paleoclimatology®

RESEARCH ARTICLE

10.1029/2024PA004855

Key Points:

- Orbital-scale variations in magnetic susceptibility resemble those in benthic foraminiferal $\delta^{18}\text{O}$ and provide orbital-scale age control
- Biogenic silica lacks a consistent response to precession between 1.1 and 2.6 Ma; obliquity-scale variability begins at 1.8 Ma
- Results support that lack of more pronounced precession in early Pleistocene $\delta^{18}\text{O}$ records may not be solely due to a muting of the signal

Correspondence to:

K. Billups,
kbillups@udel.edu

Citation:

Billups, K., Münch, B., Garrioch, I., & Bradtmiller, L. (2024). Obliquity dominance in early Pleistocene sediments from the Antarctic zone of the southern ocean (Indian Ocean sector). *Paleoceanography and Paleoclimatology*, 39, e2024PA004855. <https://doi.org/10.1029/2024PA004855>

Received 23 JAN 2024
Accepted 8 MAY 2024

Obliquity Dominance in Early Pleistocene Sediments From the Antarctic Zone of the Southern Ocean (Indian Ocean Sector)

K. Billups¹ , B. Münch^{1,2}, I. Garrioch³ , and L. Bradtmiller³ 

¹School of Marine Science and Policy, University of Delaware, Lewes, DE, USA, ²Department of Earth and Environmental Sciences, Boston College, Chestnut Hill, MA, USA, ³Department of Environmental Studies, Macalester College, Saint Paul, MN, USA

Abstract We constructed a record of percent biogenic silica (opal) accumulation at Ocean Drilling Program Site 745B located in the Indian Ocean sector of the Antarctic Zone of the Southern Ocean. The record spans the majority of the early Pleistocene (1.1–2.6 Ma). Orbital-scale sampling affords a look at the relative importance of obliquity versus precession variability through a time interval that is characterized by obliquity pacing in early Pleistocene $\delta^{18}\text{O}$ records. Variations in the site's magnetic susceptibility record closely resemble those in the benthic foraminiferal $\delta^{18}\text{O}$ stack (Lisiecki & Raymo, 2005, <https://doi.org/10.1029/2004pa001071>) and provide orbital-scale age control. Between 1.1 and 1.8 Ma, obliquity-related 41 kyr spectral peaks dominate with relatively little power at precession periods (23–19 kyr) in all records. Between 1.8 and 2.6 Ma, only the $\delta^{18}\text{O}$ and magnetic susceptibility data display a distinct 41 kyr peak, while the opal lacks spectral power at any of the orbital periodicities. The lack of more pronounced precession-scale variations in the two proxy records is consistent with observations in foraminiferal $\delta^{18}\text{O}$ records. A low or absent response to precession in these records appears to be due to environmental control. Lack of orbital forcing in the opal record before 1.8 Ma may reflect both a more southerly location of the polar frontal zone with respect to the site, and thus the site's position outside the region of wind-driven upwelling, and/or upwelling waters undersaturated with respect to silica prior to the establishment of the opal belt at about 2 Ma.

1. Introduction

1.1. Early Pleistocene Climate Cycles

Foraminiferal $\delta^{18}\text{O}$ records are the most commonly used tool to reconstruct aspects of global climate change. Because of the relatively small temperature component in the signal in benthic foraminifera, on time-scales resolvable by deep sea sediments, these records reflect global changes in the relative size of continental ice sheets and hence “global ice volume.” To the extent that global ice volume is a measure of the large-scale glacial to interglacial climate background, these records provide a continuous link between external climate forcing and response (e.g., Ahn et al., 2017; Berger, 1988; Hays et al., 1976; Imbrie et al., 1992; Lisiecki & Raymo, 2005). Specifically, foraminiferal $\delta^{18}\text{O}$ records display variations that have been related directly to the amount and distribution of insolation received due to changes in the degree of the Earth's axis tilt (obliquity) and wobble (precession) and more indirectly to eccentricity via this parameter's effect on the amplitude of precession (e.g., Hays et al., 1976; Imbrie et al., 1984, 1992). Two phenomena recorded by foraminiferal $\delta^{18}\text{O}$ records deviate from this rather linear response. One, the emergence of a 100 kyr periodicity in later Pleistocene records, and two, the lack of a more significant precession response during a portion of the early Pleistocene (~1–2 Ma), the latter being the focus of this particular study.

A number of hypotheses have been put forth to explain the relatively low response of early Pleistocene $\delta^{18}\text{O}$ records at precessional periodicities despite the fact that insolation is dominated by precession, at least at latitudes important for ice growth and decay and during the critical summer season (e.g., Imbrie et al., 1992 for a review). Explanations involve, for example, the dominance of the obliquity signal in variations of meridional insolation gradients and associated heat transport and by extension continental ice sheet size (e.g., Raymo & Nisancioglu, 2003). Another insolation-linked idea suggests that climate change is responding to the integrated summer insolation, which varies with obliquity (Huybers, 2006). Neither of these theories explains why precession should be less significant only during some intervals in the geologic record (e.g., between ~1 and 2 Ma) and not during

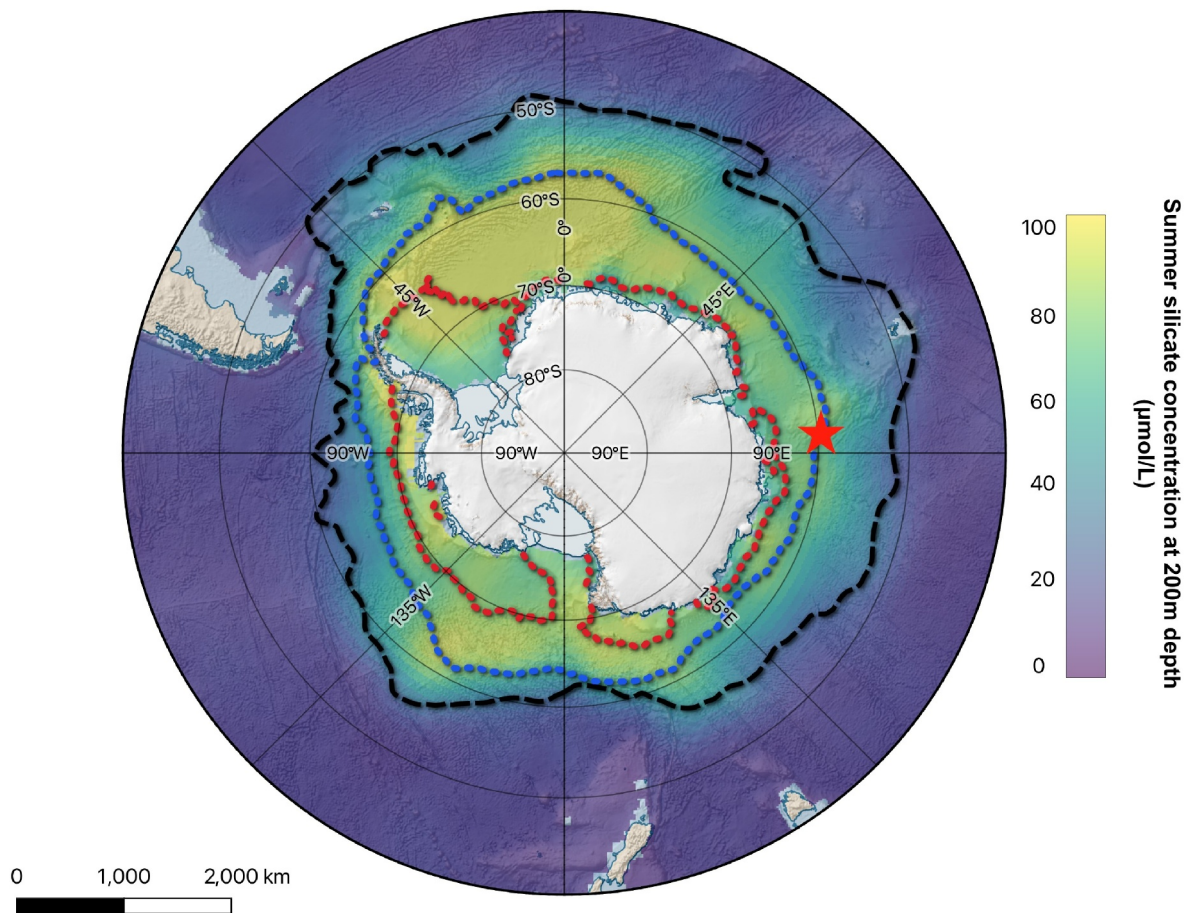


Figure 1. Location of ODP Site 745B in the Indian Ocean sector of the Antarctic Zone of the Southern Ocean (red star). The position of the modern polar front is indicated by the dashed black line (Orsi et al., 1995), and the modern sea ice extent is indicated by the dotted lines (January: red dotted line; July: blue dotted line; Fetterer et al., 2016). Colors represent summer silicate concentrations at 200m water depth (Garcia et al., 2014). The figure was generated with Quantarctica 3.2 (Matsuoka et al., 2018).

others. In a different vein, dominance in obliquity forcing in early Pleistocene $\delta^{18}\text{O}$ records has been ascribed to a lack of a more significant precession signal due to its out of phase effect on insolation, and hence ice volume, in the northern versus southern hemispheres (Raymo et al., 2006). Recent statistical re-analysis of high resolution foraminiferal $\delta^{18}\text{O}$ records from the North Atlantic, however, finds a more significant precession component in the $\delta^{18}\text{O}$ variability as previously observed (Liataud et al., 2020).

Proxies recording regional climate variability should still vary on precessional timescales if global records such as foraminiferal $\delta^{18}\text{O}$ values (or other sea level indicators) are affected by the interhemispheric asymmetry of the forcing in this band. For example, there is significant precessional variability in early Pleistocene records of low latitude eolian dust in Atlantic Ocean sediments (DeMenocal, 1995) and terrigenous inputs to the Timor Sea (Zhang et al., 2023). Furthermore, early Pleistocene mid latitude loess records contain significant precessional variability (Sun et al., 2006). On the other hand, some high latitude sea surface temperatures lack significant precession cycles during the early Pleistocene in the Northern Hemisphere (Ruddiman et al., 1989). Records of ice rafted debris display a response to precession in the Northern Hemisphere (Barker et al., 2022), but not in the Southern Hemisphere (e.g., Starr et al., 2021). These observations support the idea that the periodicities recorded by proxies reflect regionally specific expressions of the climate system and are therefore not unequivocal evidence that global climate is varying predominantly on obliquity timescales.

Here we investigate whether or not early Pleistocene proxy records in the Antarctic Zone of the Indian Ocean sector of the Southern Ocean are dominated by a 41 kyr signal. We generated a biogenic silica (opal) record from Ocean Drilling Program, ODP, Leg 113 Site 745B (Figure 1). The record fully encompasses the early Pleistocene

interval of 41 kyr dominance through the beginning of the mid Pleistocene transition toward higher amplitude 100 kyr variability (2.60–1.1 Ma, Marine Isotope Stages, MIS 103–31). The proportion of opal in the sediments is commonly interpreted as a measure of export primary productivity and therefore wind-driven changes in upper ocean stratification (e.g., Anderson et al., 2009; Charles et al., 1991; Francois et al., 1997). Late Pleistocene orbital-scale biogenic silica records at this site display significant precession variability consistent with the dominance of austral summer insolation in the latitude band of the Antarctic Zone and related westerly wind stress and upwelling (Kaiser et al., 2021). The early Pleistocene record affords a view of how consistent such variations are through time as variations in the global $\delta^{18}\text{O}$ record change from a dominant 41 kyr pattern through the onset of 100 kyr climate cycles during the mid Pleistocene transition.

1.2. Site Location

ODP Site 745, Hole B, (59°37'S, 85°52'E, 4,082 m water depth) lies in the Indian Ocean sector of the Antarctic Zone of the Southern Ocean (e.g., Figure 1). In this region, cold deep water upwells keeping sea surface temperatures below 1.8°C even during the summer months. At almost 60°S, the site is well to the north of the modern summer sea-ice boundary (e.g., Cavalieri & Parkinson, 2008), which is the season that is critical for primary productivity in this region. On longer time scales, cores to the east of Site 745B suggest that this region was just north of the summer sea ice boundary during the Last Glacial Maximum (Gersonde et al., 2005). Therefore, a priori, variations in Site 745 biogenic silica can be interpreted with respect to export productivity related to wind-driven upwelling rather than sea ice cover (e.g., Hillenbrand and Cortese (2006); Tang et al., 2016; Wu et al., 2017).

1.3. Sedimentary Regime

The sedimentary regime at Site 745 reflects the sensitivity of this region to paleoenvironmental changes. Pleistocene sediments consist of biogenic silica (opal, primarily diatoms, on average 40%) and terrigenous material (clays, ~60% and some ice rafted debris) with very little carbonate (<1%) (Ehrmann et al., 1991; Ehrmann & Grobe, 1991). Percent opal in the sediments increases to on average above 50% at about 2 Ma (Ehrmann et al., 1991), which is consistent with increases in opal at other Southern Ocean sites, reflecting the establishment of the modern-type silica belt in this region (Cortese et al., 2004). Similar to the late Pleistocene, early Pleistocene variations in the relative amount of biogenic silica versus terrigenous sediments are attributed to glacial/interglacial climate patterns with generally higher biogenic silica content during interglacial intervals and higher, Antarctic-sourced, terrestrial sediments during glacial intervals (Ehrmann & Grobe, 1991; Kaiser et al., 2021).

2. Methods

2.1. Sampling

We sampled 1 cc of bulk sediment every 10 cm from 54.28 m below sea floor (mbsf) to 112.38 mbsf. This extends the bottom of the published portion of the record (~1.1 Ma, Billups et al., 2018) through the entire early Pleistocene (2.6 Ma). The sampling interval is the same as in the published records and results in a similar temporal resolution of 2–3 kyr (Billups et al., 2018; Kaiser et al., 2021), which is sufficient to fully resolve variations related to orbital forcing (e.g., precession cycles at 6–9 data points per cycle). The section, which spans seven cores, is complete with a 100% recovery (Shipboard Scientific Party, 1989).

2.2. Biogenic Silica Extraction

Biogenic silica was extracted from bulk sediments using the standard procedure of Mortlock and Froelich (1989). About 50 mg of samples were freeze-dried, and then crushed with an agate pestle. Carbonates and organic materials were chemically dissolved, and biogenic silica was extracted in a NaOH bath. An empty centrifuge tube (a blank) was used to identify potential contamination of samples, and a sample was used in order to rule out long-term drifts. Biogenic silica was measured using molybdate-blue spectrophotometry at the University of Delaware and Macalester College. Concentrations were calculated by comparing the measured sample absorbance (averaged between two mixing bottles per sample) to a standard curve with concentrations from 0 to 14 mM. The interlaboratory offset is $0.87 \pm 3.9\%$ (Kaiser et al., 2021). The reproducibility of the silica measurements in the present study is $4 \pm 2\%$ ($n = 7$).

2.3. Time Series Analysis

We used QAnalySeries (Kotov & Pälike, 2018) and the Arand software package (Howell, 2012) for the derivation of the orbital-scale age model and to confirm significance of orbital periodicities. All records ($\delta^{18}\text{O}$, magnetic susceptibility, percent opal) were interpolated to a constant 2 kyr time step in keeping with the average resolution of the opal data and then linearly detrended. For cross-spectral analysis of $\delta^{18}\text{O}$ and magnetic susceptibility to test the age model, we used 120 lags specifying a 95% confidence interval. For spectral analysis on individual time intervals, we used 90 lags and a confidence interval of 95%. Evolutive spectra were conducted on the entire 2.6 myr long record afforded by appending the late Pleistocene opal record from Kaiser et al. (2021). Analyses were conducted using the Acycle software package by Li et al. (2019). All evolutive spectral analyses are based on the Fast Fourier transform method by Kodama and Hinnov (2015), using sliding window size and time step parameters aimed at resolving orbital-scale variability. While the respective values differ slightly between analyses, a window size of ~ 520 kyr and a time step of ~ 4.16 kyr were selected.

2.4. Mass Accumulation Rates

We calculated opal mass accumulation rates (MAR) in order to confirm that variations in the record are related to productivity changes, and, in this two-component system, are not simply driven by variations in terrigenous fluxes. Our approach to constrain the dry bulk density follows Kaiser et al. (2021) who apply a correction factor to the continuous GRAPE density based on the difference between it and discrete shipboard dry bulk density (DBD) measurements (-0.79 g cm^{-3}). The difference between these two measures of DBD is the same during the early Pleistocene interval of interest here (not shown). We subtracted this value from the GRAPE record and interpolated the record to the depths of our data points. Silica MARs are then calculated by multiplying the fraction of silica in the sediments by the thus derived DBD and the sedimentation rates obtained from the orbitally tuned age model (see below). We note here that we only use the MAR record as a qualitative means to confirm that maxima and minima correspond to maxima and minima in the % biogenic silica time series. The MARs are heavily overprinted by the sedimentation rates and are therefore not symmetrical and conducive to spectral analyses.

3. Age Model

We developed an orbital-scale age model by tuning the site's magnetic susceptibility record on the depth scale (available through the Janus data base at: <http://web.iodp.tamu.edu/OVERVIEW/>) to the benthic foraminiferal $\delta^{18}\text{O}$ stack of Lisiecki and Raymo (2005) (LR04). Beginning on the depth scale, the magnetic susceptibility signal is pronounced and many of the variations mimic those displayed by the $\delta^{18}\text{O}$ composite, particularly between 68 mbsf and 80 mbsf (Figure 2). Moreover, there are a few distinct features in the magnetic susceptibility record that can also be found in the $\delta^{18}\text{O}$ record. For example, a prominent maximum in magnetic susceptibility at 98 mbsf can be matched to the prominent $\delta^{18}\text{O}$ maximum of MIS 78 (2.07 Ma). In addition, at the bottom of the record, the double peak in magnetic susceptibility between 110 and 112 mbsf can be related to MIS 101 and 103 (~ 2.5 – 2.6 Ma).

To investigate if there is a dominant primary periodicity in these variations, we conducted a spectral analysis on the depth scale (Figure 3). We broke the record into two segments at 89 mbsf due to a change in the sedimentation rate apparent in the ages derived from the site's paleomagnetic reversal pattern (Sakai & Keating, 1991) (Table 1). The sedimentation rate change is robust regardless of the time scale applied to the reversal pattern (i.e., Sakai & Keating, 1991 or Channell et al., 2016, Table 1). The depth spectrum of the younger interval (54–89 mbsf) is clearly dominated by a peak with a wavelength of about 2.5 m. The depth spectrum in the older time interval (89–112 mbsf) has significant concentration of power at 0.8 m, plus additional peaks at longer and shorter frequencies giving the spectrum a more typical red noise appearance. Applying paleomagnetic age-derived sedimentation rates of $\sim 6 \text{ cm kyr}^{-1}$ during the younger interval and $\sim 2 \text{ cm kyr}^{-1}$ during the older (e.g., Table 1), the significant peaks have periodicities of about 40 kyr in the younger time interval and 400, 80, 40, and 29 kyr in the older one. Thus, it is apparent that variations in the magnetic susceptibility record display significant variations on obliquity time scales. Because these periodicities are present in the raw data, we conclude that tuning this record to the $\delta^{18}\text{O}$ stack brings into focus the temporal variations but does not artificially introduce them. We note that the paleomagnetic reversal record at Site 745 implies low sedimentation rates of $\sim 1 \text{ cm kyr}^{-1}$ during the 150 kyr duration of the Olduvai (Table 1). This observation questions the paleomagnetic reversal pattern as an independent check on the tuned age model for this particular interval of time.

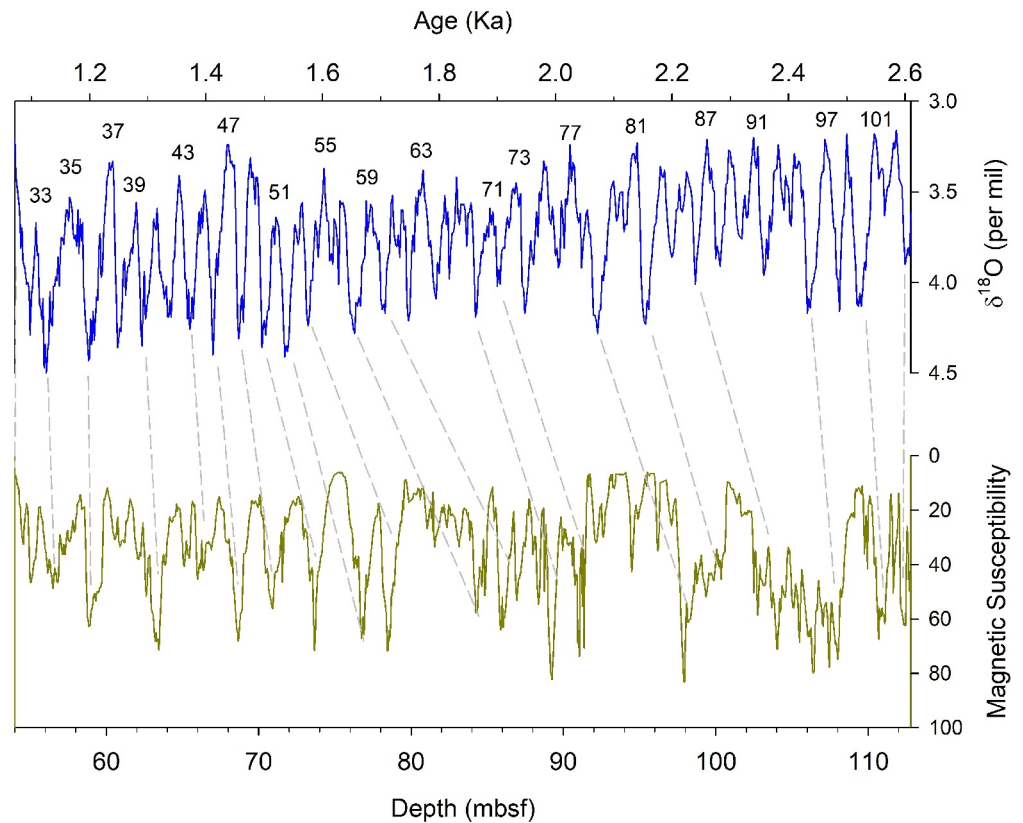


Figure 2. Comparison between (a) the LR04 $\delta^{18}\text{O}$ record on the age-scale and (b) magnetic susceptibility at Site 745B on a depth-scale (meters below sea floor, mbsf). Vertical dashed lines indicate the position of first order age model tie points between the $\delta^{18}\text{O}$ record and magnetic susceptibility. Numbers refer to interglacial Marine Isotope Stages (MIS) following the definition of Lisiecki and Raymo (2005). The age-depth axes were scaled such that the top and bottom of the section correspond to known age model control points from Kaiser et al. (2021) (53.68 mbsf-1.068 Ma) and the Matuyama-Gauss boundary (112.3 mbsf-2.608 Ma).

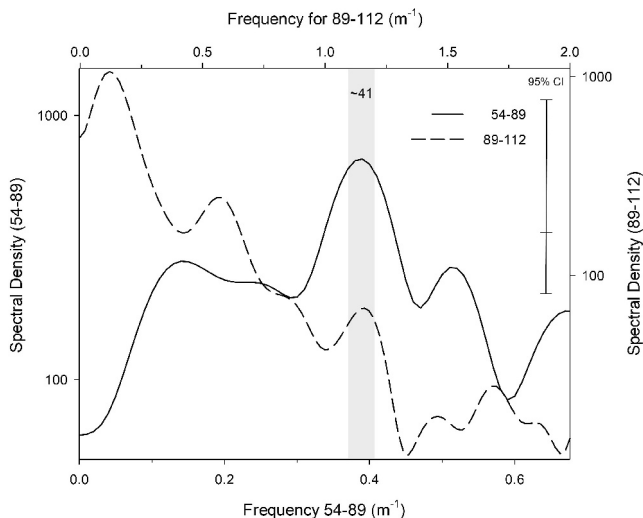


Figure 3. Power spectrum of the magnetic susceptibility record on the depth scale 54–89 mbsf (solid line) and 89–112 mbsf (dashed line) in line with the change in sedimentation rates at this depth (Table 1). Using sedimentation rates derived from the paleomagnetic reversal pattern at this site (see text and Table 1) indicates that the peak at 2.5 m in the younger and 1.25 m in the older corresponds to the obliquity periodicity of about 41 kyr.

We first aligned the magnetic susceptibility to the $\delta^{18}\text{O}$ record using the major tie points shown in Figure 2. This age model is then “fine-tuned” by aligning less pronounced features using QAnalyzeSeries (Kotov & Pälike, 2018) to obtain orbital-scale depth-age control points (Table 2). Cross-spectral analysis between these two time series confirms the tuning strategy (Figure 4). During the study interval (1.1–2.6 Ma), the $\delta^{18}\text{O}$ record exhibits a dominant peak in the obliquity band, as well as a significant but comparatively weak power in the precession band (23–19 kyr, Figure 4a). The tuned magnetic susceptibility record exhibits these same spectral characteristics, with larger spectral density in the obliquity than the precession band. The two records are coherent above the 95% level (Figure 4b). In further support of the tuning strategy, the two records are essentially in phase (0.1 ± 1.3 kyr and 1.3 kyr ± 1.7 kyr at the 41 and 23 kyr periodicities, respectively, Figure 4c).

Comparison of the 41 and 21 kyr bandpass filters of the two records illustrates the fit on the scale of individual cycles and their amplitude modulation (Figures 4d and 4e). At the 41 kyr periodicity, variations in the filter output show a remarkable degree of correspondence in both pacing and amplitude. There is some disagreement between ~ 2.1 Ma and 2.2 Ma when the amplitude of the magnetic susceptibility filter output is notably smaller than the amplitude of the $\delta^{18}\text{O}$ filter output. The low amplitude variations in magnetic susceptibility are apparent in the original time series, which displays an

Table 1
 Summary of Paleomagnetic Reversal Sequence at Site 745 (Sakai & Keating, 1991)

Chron	Mbsf	Age ^a (Ma)	Sed rates ^a (cm kyr ⁻¹)	Age ^b (Ma)	Sed rates ^b (cm kyr ⁻¹)
Jaramillo (b)	54.3	0.94		1.07	
Gilsa	89.55	1.62	5.18	1.584	6.86
Olduvai (t)	91.8	1.76	1.61	1.78	1.15
Olduvai (b)	93.3	1.91	1.00	1.925	1.03
Reunion (t)	99.3	2.07	2.42	2.116	3.14
Matuyama (b)	112.3	2.47	3.39	2.595	2.71

^aSakai and Keating (1991). ^bChannell et al. (2016).

increase in values between 98 and 100 mbsf with very little superimposed variability (e.g., Figure 2, bottom panel). The 21 kyr filter output of the two records also shows excellent agreement. Given that the record was tuned using primarily 41 kyr spaced maxima in the records, the agreement in the 21 kyr output is an additional confirmation of the tuning strategy.

4. Results

It has been well established that during the early Pleistocene, glacial-interglacial $\delta^{18}\text{O}$ cycles are dominated by the 41 kyr obliquity periodicity. As evident in the LR04 $\delta^{18}\text{O}$ time series, the amplitude and precise pacing of these cycles varies somewhat throughout the study interval (Figure 5a). Obliquity-scale cycles are particularly well expressed in the time series between ~ 1.1 and 1.6 Ma, but are less regular and of smaller amplitude between ~ 1.6 and 2.4 Ma, and gain amplitude again between ~ 2.4 and 2.5 Ma.

Throughout the entire study interval, the glacial-interglacial variability described by the $\delta^{18}\text{O}$ stack can also be found in the magnetic susceptibility record (Figure 5b) making it an ideal tuning medium as argued above. The similarities between the $\delta^{18}\text{O}$ and magnetic susceptibility record are remarkable during the 1.1–1.6 Ma interval when the $\delta^{18}\text{O}$ variations are of high amplitude, a pattern that is particularly well expressed in the 41 kyr filter output (Figure 4d). Between 1.9 and 2.4 Ma (MIS 71–95), individual magnetic susceptibility cycles match $\delta^{18}\text{O}$ variability, but magnetic susceptibility also displays longer term amplitude modulation not seen in the $\delta^{18}\text{O}$ record. Furthermore, and as noted above in the context of evaluating the 41 kyr filter output (Figure 4d), between MIS 83 and toward the glacial maximum defined by MIS 78, magnetic susceptibility increases but displays only very small amplitude variations. At the bottom of the record (MIS 97–103), the character of the magnetic susceptibility again matches the $\delta^{18}\text{O}$ record very well.

Sedimentation rates resulting from the tuned age model are relatively constant varying between ~ 2 and ~ 6 cm kyr⁻¹ on average (Figure 5c) consistent with sedimentation rates during the late Pleistocene (Kaiser et al., 2021). There is one interval of particularly low rates (0.4 cm kyr⁻¹) during MIS 71 (1.87–1.91 Ma), and one interval of sustained high rates (10 cm kyr⁻¹) during MIS 54–56 (1.58–1.63 Ma). Relatively smoothly varying sedimentation rates support the tuning strategy.

Percent biogenic silica (opal) displays maxima during intervals of low $\delta^{18}\text{O}$ values and minima during intervals of high $\delta^{18}\text{O}$ values, particularly after 1.8 Ma when the amplitude of the variations becomes more pronounced (Figure 5d). This observation is in excellent agreement with the general observations from this site that biogenic silica accumulation is high during warm interglacial and low during cold glacial intervals, essentially the opposite of terrigenous inputs, in support of a two-component sediment system (Ehrmann

Table 2
 Depth-Age Control Points for Site 745 Based on Tuning to LR04

Mbsf	Age (Ka)	Mbsf	Age (Ka)	Mbsf	Age (Ka)
55.05	1,098.0	86.95	1,747.5	100.35	2,200.0
56.50	1,122.0	87.75	1,772.5	100.85	2,212.5
58.85	1,198.0	88.35	1,795.0	101.55	2,225.0
60.05	1,238.0	88.75	1,812.5	102.75	2,240.0
60.90	1,250.0	89.75	1,830.0	104.05	2,282.5
61.60	1,260.0	90.05	1,837.5	104.75	2,297.5
63.45	1,290.0	91.05	1,862.5	105.15	2,320.0
65.05	1,334.0	91.20	1,900.0	105.50	2,330.0
66.00	1,368.0	92.05	1,947.5	105.65	2,340.0
68.65	1,415.0	94.10	1,982.5	106.35	2,357.5
70.85	1,460.0	94.50	2,005.0	106.75	2,382.5
73.65	1,501.0	96.20	2,045.0	107.45	2,405.0
76.75	1,541.0	97.95	2,072.5	107.9	2,437.5
78.50	1,579.0	98.35	2,087.5	109.95	2,487.5
79.85	1,592.5	98.55	2,105.0	110.7	2,517.5
81.55	1,612.5	98.75	2,117.5	111.10	2,532.5
83.15	1,627.5	99.05	2,137.5	111.50	2,547.5
84.35	1,653.0	99.35	2,155.0	111.65	2,565.0
86.00	1,705.0	100.15	2,187.5	112.40	2,607.5

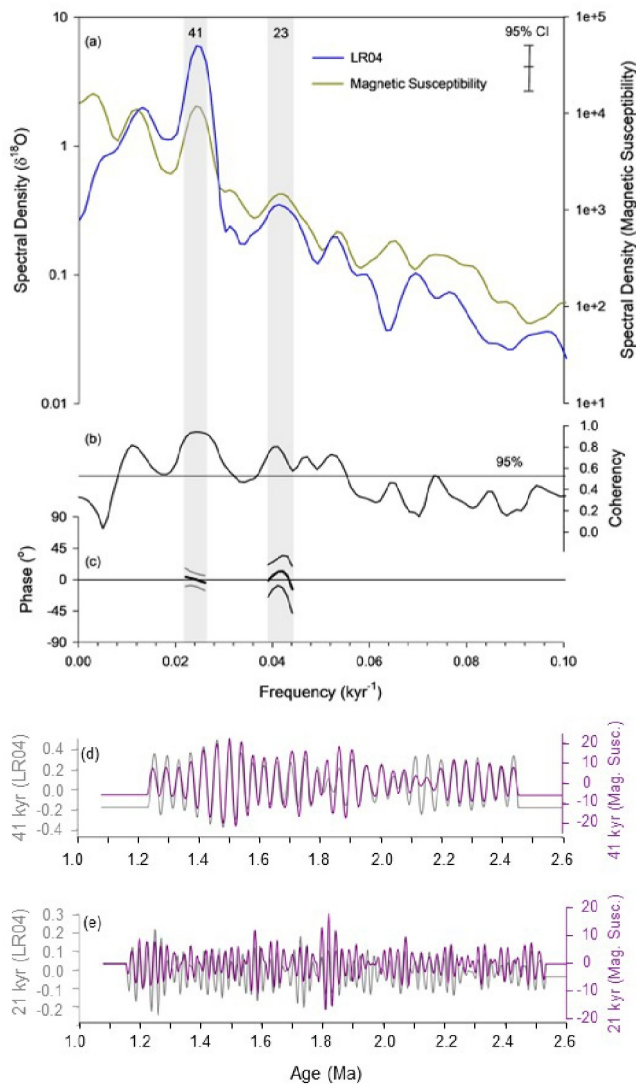


Figure 4. Cross-spectral analysis between the LR04 $\delta^{18}\text{O}$ stack (multiplied by -1 to reference interglacial conditions) and magnetic susceptibility (a); coherency of the two records (b) using a 95% test statistic; and phase relationship at the 41 and the 23 kyr periodicity with the average represented by the bold lines and the phase error represented by gray lines (c). The vertical gray bars demarcate the primary orbital periodicities. Panels (d) and (e) illustrate the comparison of the obliquity (centered on 41 kyr), and precession (centered on 21 kyr) filter outputs, respectively, of the target and the tuning medium. Analyses were conducted using the Arand software package (Howell, 2012).

between 2.6 and 1.8 Ma, but clearly and continuously dominates between 1.8 and 1.2 Ma (Figure 6b). With the exception of this particular time interval, longer term periodicities are intermittently present throughout the record including a distinct 100 kyr cycle after 0.7 Ma. The percent opal record (used here due to the asymmetrical nature of the MARs as noted above) displays relatively high 41 kyr power continuously between about 1.8 and 0.7 Ma (Figure 6c). As in the magnetic susceptibility data, longer periodicities are apparent intermittently throughout the record.

Focusing on our study interval (1.1–2.6 Ma), the evolutive spectra of the proxy records summarize that while the $\delta^{18}\text{O}$ record displays continuous response to obliquity forcing, there are two distinct intervals of time characterized by differing orbital scale variations in the other proxy records. Between 1.1 and 1.8 Ma, obliquity variations are continuous in both magnetic susceptibility and opal, but between 1.8 and 2.6 Ma

& Grobe, 1991; Kaiser et al., 2021). The long-term trend in the percent opal parallels the long-term trend in the magnetic susceptibility, and those features where the magnetic susceptibility deviates from the $\delta^{18}\text{O}$ record are also apparent in the opal (e.g., low variability between MIS 83–79, longer-term maximum between MIS 77–71). In fact, the abrupt transition between one of the more extreme glacial maxima (MIS 78) to the more pronounced interglacial MIS 77 is recorded by both proxies with an amplitude that exceeds any of the other changes recorded as well as the relative amplitude in the $\delta^{18}\text{O}$ record.

Over the long term, opal MARs (Figure 5e) are strongly modulated by the sedimentation rate multiplier as evident in the similarity of the asymmetry of the two records. On the scale of individual cycles, however, opal MARs resemble the pattern found in the percent opal record, with generally higher opal MARs during interglacial and lower MARs during glacial periods. This relationship is particularly apparent during the MIS 78/77 transition (deglaciation) when the percent opal rapidly increases. Opal MARs remain comparatively high between MIS 78 and MIS 73, with another prominent peak during MIS 74–75 coinciding with high percent opal. As one would expect, during the percent opal and sedimentation rates minimum of MIS 71, opal MARs take on values close to zero. As the magnetic susceptibility maximum at this time is also relatively low, this would be indicative of relatively low amounts of terrigenous sediment. Thus, low sedimentation rates during this time point to an environmental origin rather than an age model artifact. Overall, the opal MARs confirm that variations in % biogenic silica are not simply driven by fluctuations in the terrigenous sediment component as recorded by the magnetic susceptibility, but the signal is relatively small ($0.1\text{--}1.3\text{ g cm}^{-2}\text{ kyr}^{-1}$) prior to 2.1 Ma. In fact, late Pleistocene opal MARs minima of $\sim 0.5\text{ g cm}^{-2}\text{ kyr}^{-1}$ and maxima of $>2\text{ g cm}^{-2}\text{ kyr}^{-1}$ are not reached until after 1.62 Ma (with the exception of a singular maximum during MIS 78 at 2.05 Ma).

Evolutive spectra provide further information regarding overall changes in the amplitude and pacing of the orbital-scale variations recorded by the records (Figure 6). For this purpose we show the records for the entire Pleistocene time interval, which necessitated appending the published record of Kaiser et al. (2021) at 1.1 Ma. We note that the age model of the records in the younger interval are based on tuning the opal record to LR04 as it provided a clearer signal. The evolutive spectrum of the $\delta^{18}\text{O}$ record confirms the dominance of 41 kyr variations between 2.6 Ma until about 0.7 Ma (Figure 6a). Longer periodicities are also present in the earlier part of the record and after 1.1 Ma. Between about 1.8 and 1.1 Ma, however, the spectrum is dominated by a singular periodicity at 41 kyr. At 0.7 Ma, a well-defined, 100 kyr periodicity begins to dominate the spectrum. In the magnetic susceptibility spectrum, the 41 kyr periodicity is present intermittently

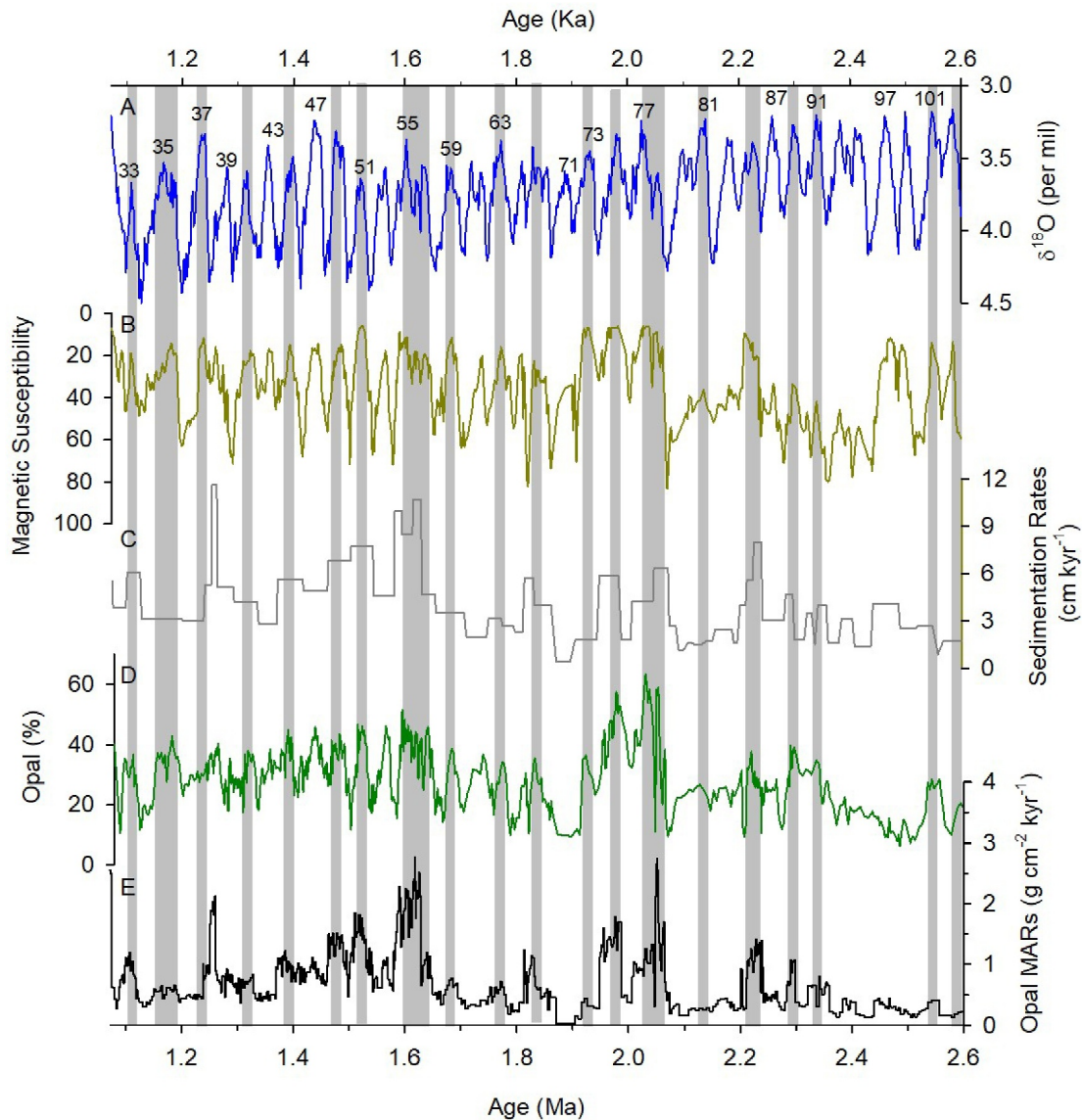


Figure 5. Comparison of the LR04 $\delta^{18}\text{O}$ stack (a) with the tuned magnetic susceptibility record (b), the resulting sedimentation rates (c), percent biogenic silica (d), and biogenic silica mass accumulation rates (MAR) (e). Note the inverted y axis in (b) to visually align minima in the record with maxima in percent opal in panel (d). Select interglacial intervals are labeled across the top and highlighted with gray bars.

orbital-scale variations are only intermittently apparent in the magnetic susceptibility and weak or absent in the opal record.

Spectral analysis conducted on these two time intervals provides a better resolved comparison of the precise periodicities and relative amplitude in these records (Figure 7). During the 1.1–1.8 Ma interval, $\delta^{18}\text{O}$, magnetic susceptibility, and % opal display a distinct, dominant 41 kyr peak (Figure 7a). Distinct concentration of spectral density at the precessional periodicities is markedly less, but significant above the 95% level in the 23 and 19 kyr band in the $\delta^{18}\text{O}$ record, the 23 kyr band in the magnetic susceptibility record, and questionably in the 19 kyr band in the magnetic susceptibility and opal records. Between 1.8 and 2.6 Ma, a dominant 41 kyr obliquity peak is significant in the $\delta^{18}\text{O}$ and magnetic susceptibility records; no significant spectral power at any orbital periodicities is evident in the opal data (Figure 7b). The $\delta^{18}\text{O}$ and magnetic susceptibility do not resolve individual precessional peaks, spectral power occurs in a relatively broad band between about 19 and 33 kyr.

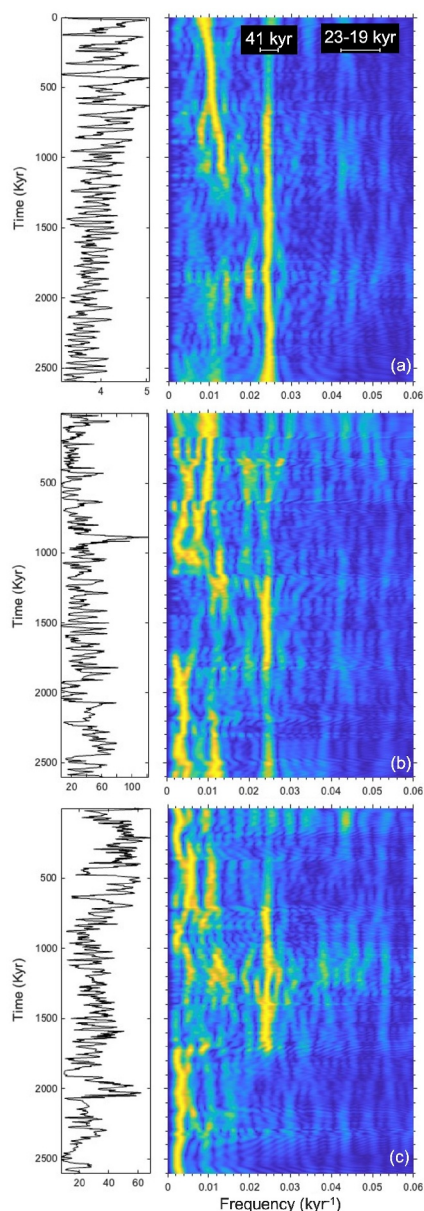


Figure 6. Evolutive spectral analysis of (a) LR04 $\delta^{18}\text{O}$ stack, (b) magnetic susceptibility and (c) percent opal record at Site 745B from 2.6 Ma to present (0–1.1 Ma is from Kaiser et al., 2021). Left panels show the respective time-series, right panels display normalized spectral density on a parula color scale from dark blue (i.e., 0) to yellow (i.e., 1). All analyses were conducted using the Acycle software package (Li et al., 2019) and the Fast Fourier transform method by Kodama and Hinnov (2015). Sliding window size and time step parameter were adjusted to target orbital-scale variability. The time step is 4.16 kyr.

suggests that productivity is driven by a forcing that does not vary on the precessional scale (including dilution by terrigenous sediments on these timescales as these do display a precession signal). For example, upwelling could be driven by meridional changes in the axis of maximum westerly wind stress as set by the latitudinal temperature gradient determined either by variations in high latitude insolation or ice extent. As is the case for the magnetic susceptibility record, we cannot think of a mechanism that would mute biogenic silica sedimentation on precessional time scales.

5. Discussion

5.1. Magnetic Susceptibility-The Tuning Medium

Results evidence the importance of obliquity forcing in the magnetic susceptibility record during the early Pleistocene throughout the entire study interval. The close relationship between magnetic susceptibility and the $\delta^{18}\text{O}$ record, which is apparent in the depth domain (Figure 3), makes this proxy an ideal tuning medium and indicates a close relationship between ice volume and terrigenous sedimentation at Site 745. The similarity of the spectral character of this record with the $\delta^{18}\text{O}$ spectrum, as opposed to the opal spectrum (e.g., Figure 7), supports a more direct relationship with ice volume rather than a result of dilution by opal (e.g., Figure 7). Variations in terrigenous sedimentation at this site reflect variations in terrigenous fluxes due to erosion and transport processes in the source region, the continental margin of Antarctica, or variations in bottom water current strength at the site (e.g., winnowing) (Ehrmann & Grobe, 1991). In either case, the strong response to obliquity indicates that variations in terrigenous sedimentation varies at the same scale as the ice volume record and is likely driven by it either directly via growth and decay of the ice sheet and associated variations in terrigenous fluxes or more indirectly via climate-linked changes in bottom water circulation. We argue against a wind-driven input of terrigenous clays to the region as a dominant mechanism producing variations in magnetic susceptibility because Site 745 is not underneath the path of major dust plumes originating in South America, Africa, or Australia (Li et al., 2008). While this may not preclude that the region remained entirely “dust free” on glacial to interglacial time-scales, the amount of dust reaching the site is presumably relatively small. Regardless of the mechanism that controls terrigenous sedimentation at Site 745, the close relationship between magnetic susceptibility and the benthic foraminiferal $\delta^{18}\text{O}$ record does not lend support to the hypothesis that the precession signal is muted in the $\delta^{18}\text{O}$ record due to the effect of insolation on ice sheet variations, which are hemispherically out of phase and would cancel (Raymo et al., 2006). There is no conceivable mechanism that would cancel out precession in the magnetic susceptibility record.

5.2. Biogenic Silica-Biological Productivity

Dominance of the obliquity signal in the percent opal record between 1.1 Ma and 1.8 Ma together with the lack of more pronounced precession variability also supports a control of an obliquity-paced Antarctic ice sheet on Southern Ocean hydrography. Specifically, this prominence of obliquity in the productivity proxy might be explained by a direct response of upwelling related to shifts in the westerly wind belt due to changes in the latitudinal temperature gradient either forced at the high latitude end by the growth and decay of the Antarctic ice sheet, or by high latitude insolation gradients. As the opal record is phase locked to the $\delta^{18}\text{O}$ record due to the tuning strategy, it is not possible to distinguish between the two mechanisms on the basis of their inherent system response time. In any case, the dominance of the 41 kyr periodicity and lack of more pronounced precession in the opal between 1.1 and 1.8 Ma

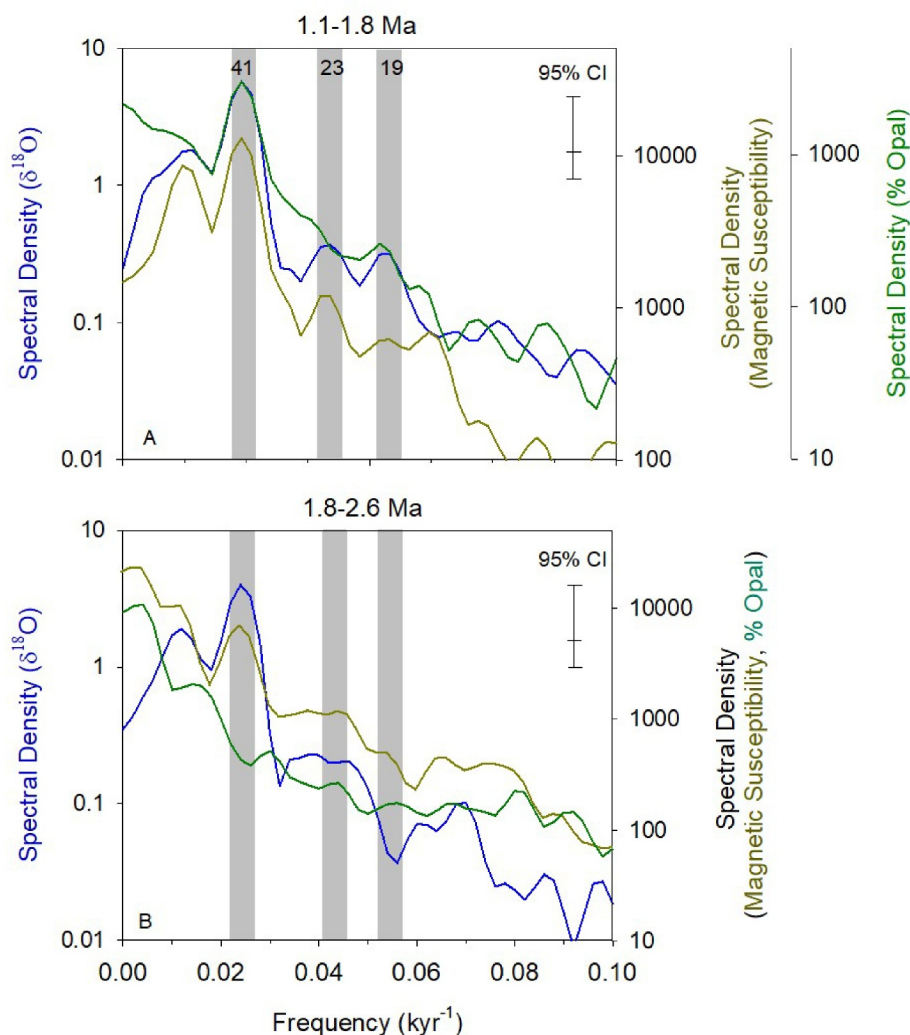


Figure 7. Spectral analysis of LR04 $\delta^{18}\text{O}$ (blue), magnetic susceptibility (dark yellow) and percent opal (green) for two time intervals (a) 1.1–1.8 Ma, (b) 1.8–2.6 Ma. Gray boxes indicate obliquity (i.e., 41 kyr) and precession (i.e., 23 and 19 kyr) periodicities as recorded by the $\delta^{18}\text{O}$ record. Analysis was conducted using the Arand software package (Howell, 2012), see text for details.

The rise of orbital-scale variability in the percent opal at about 1.8 Ma coincides with the increase in average sedimentation rates and an increase in the percent biogenic silica in the sediments, and hence its accumulation rate (e.g., Figures 5c–5e, respectively). This change follows the pulse in opal sedimentation at 2.05 Ma. The timing of this pulse is consistent with similar increases in opal sedimentation in the Southern Ocean and reflects the establishment of the Southern Ocean opal belt (e.g., Cortese et al., 2004). Thus, it is likely that these events are related. Although sedimentation rates are low prior to 1.8 Ma, they are high enough ($\sim 2 \text{ cm kyr}^{-1}$) to fully resolve potential 41 kyr obliquity cycles. Thus, we rule out that low sedimentation per se is the reason for the lack of orbital-scale variability in the percent opal record prior to 1.8 Ma.

Several environmental changes took place at Site 745 at around 2 Ma that suggest that the polar frontal zone moved north above Site 745 at about this time. Not only is the percent biogenic silica above 50% for the first time at 2 Ma, this increase is similar to the pattern observed at Southern Ocean sites to the north, but not to the south of Site 745 (Billups et al., 2013). This observation is consistent with the hydrography at Site 745 having been more similar to the sites to the north and hence a more southerly location of the polar frontal zone (Billups et al., 2013). In addition, $\delta^{15}\text{N}$ values of bulk sediments begin to be inversely related to, albeit on longer than orbital time-scales, variations in the corresponding silica record, indicating the beginning of a relationship between water

column stratification, nutrient utilization and export productivity (Billups et al., 2013). Thus, it may be that the beginning of orbital-scale variations at 1.8 Ma signifies that by then the site was underneath an area that is sensitive to wind-driven upwelling of relatively silica enriched waters. Since then, enhanced biogenic silica deposition is associated with interglacial intervals and vice versa, a relationship that persists through the MPT and the late Pleistocene. Both observations support a northward movement of the polar frontal zone to its modern-like position between 2 Ma and 1.8 Ma.

6. Conclusions

The dominance of obliquity variations in early Pleistocene $\delta^{18}\text{O}$ records provides a challenge to our understanding of this proxy and the response of high latitude ice sheets to insolation forcing. Here we contribute to this question with a biogenic silica record from the Indian Ocean sector of the Antarctic Zone of the Southern Ocean, ODP Site 745B. For age control, we tuned the site's magnetic susceptibility record to the benthic foraminiferal $\delta^{18}\text{O}$ stack (Lisiecki & Raymo, 2005). The approach is justified by the observation that obliquity-scale cycles are evident in the magnetic susceptibility on the depth-scale using average sedimentation rates based on the site's paleomagnetic reversal record. Results indicate that between 1.1 Ma and 1.8 Ma, obliquity-related 41 kyr spectral peaks dominate with relatively little power at precession periods (23–19 kyr) in the magnetic susceptibility and the biogenic silica. Between 1.8 and 2.6 Ma, only the $\delta^{18}\text{O}$ and magnetic susceptibility data display a distinct 41 kyr peak, the biogenic silica lacks spectral power at any of the orbital periodicities. The pronounced dominance of obliquity in all records, at least between 1.1 and 1.8 Ma is consistent with a lack of forcing on the precessional scale. Lack of any apparent orbital forcing in the opal record before 1.8 Ma, which to a large part is before the establishment of the opal belt in the Southern Ocean by about 2 Ma, supports that the site was to the north of the polar frontal zone and therefore not sensitive to orbital-scale wind-driven upwelling or that upwelled waters were undersaturated with respect to silica.

Data Availability Statement

The data presented in this study are available on the NOAA data archive (Billups et al., 2024). This research used samples collected by the Ocean Drilling Program (ODP) and provided by the International Ocean Discovery Program (IODP). ODP and IODP are sponsored by the U.S. National Science Foundation (NSF) and participating countries.

Acknowledgments

We thank the editors for handling the manuscript and Aiden Starr and an anonymous reviewer for constructive reviews that have helped us improve this contribution. Financial support for BM was provided by the School of Marine Science and Policy in the form of a Marian Okie graduate fellowship, a Stavros award for analyses, and a travel award to the Fall 2022 AGU meeting. Additional funding for BM was provided by the German Academic Exchange Service (DAAD). We thank Dr. George Luther at the University of Delaware for use of and help with the spectrophotometer.

References

- Ahn, S., Khider, D., Lisiecki, L. E., & Lawrence, C. E. (2017). A probabilistic Pliocene–Pleistocene stack of benthic $\delta^{18}\text{O}$ using a profile hidden Markov model. *Dynamics and Statistics of the Climate System*, 2(1). <https://doi.org/10.1093/climsys/dzx002>
- Anderson, R. F., Ali, S., Bradtmiller, L. I., Nielsen, S. H. H., Fleisher, M. Q., Anderson, B. E., & Burckle, L. H. (2009). Wind-driven upwelling in the southern ocean and the deglacial rise in atmospheric CO₂. *Science*, 323(5920), 1443–1448. <https://doi.org/10.1126/science.1167441>
- Barker, S., Starr, A., van der Lubbe, J., Doughty, A., Knorr, G., Conn, S., et al. (2022). Persistent influence of precession on northern ice sheet variability since the early Pleistocene. *Science*, 376(6596), 961–967. <https://doi.org/10.1126/science.abm4033>
- Berger, A. (1988). Milankovitch theory and climate. *Reviews of Geophysics*, 26(4), 624–657. <https://doi.org/10.1029/rg026i004p00624>
- Billups, K., Aufdenkampe, A., & Hays, R. (2013). Late Miocene through early Pleistocene nutrient utilization and export production in the Antarctic Zone of the Southern Ocean. *Global and Planetary Change*, 100, 353–361. <https://doi.org/10.1016/j.gloplacha.2012.11.014>
- Billups, K., Muench, B., Garrioch, I., & Bradtmiller, L. I. (2024). NOAA/WDS paleoclimatology - Biogenic silica measurements from ODP 745B in the Antarctic Zone of the Indian Ocean sector of the southern ocean spanning the early Pleistocene (1.1–2.6Ma) [Dataset]. *NOAA National Centers for Environmental Information*. <https://doi.org/10.25921/34tf-ks29>
- Billups, K., York, K., & Bradtmiller, L. I. (2018). Water column stratification in the Antarctic zone of the southern ocean during the mid-Pleistocene climate transition. *Paleoceanography and Paleoclimatology*, 33(5), 432–442. <https://doi.org/10.1029/2018PA003327>
- Cavalieri, D. J., & Parkinson, C. (2008). Antarctic sea ice variability and trends, 1979–2006. *Journal of Geophysical Research*, 113(C7), C07004. <https://doi.org/10.1029/2007jc004564>
- Channell, J. E. T., Hodell, D. A., & Curtis, J. H. (2016). Relative paleointensity (RPI) and oxygen isotope stratigraphy at IODP site U1308: North Atlantic RPI stack for 1.2–2.2 Ma (NARPI-2200) and age of the Olduvai Subchron. *Quaternary Science review*, 131(Part A), 1–19. <https://doi.org/10.1016/j.quascirev.2015.10.011>
- Charles, C. D., Froelich, P. N., Zibello, M. A., Mortlock, R. A., & Morley, J. J. (1991). Biogenic opal in Southern Ocean sediments over the last 450,000 years: Implications for surface water chemistry and circulation. *Paleoceanography and Paleoclimatology*, 6(6), 697–728. <https://doi.org/10.1029/91PA02477>
- Cortese, G., Gersonde, R., Hillenbrand, C. D., & Kuhn, G. (2004). Opal sedimentation shifts in the world ocean over the last 15 Myr. *Earth and Planetary Science Letters*, 224(3–4), 509–527. <https://doi.org/10.1016/j.epsl.2004.05.035>
- DeMenocal, P. B. (1995). Plio-Pleistocene African climate. *Science*, 270(5233), 53–59. <https://doi.org/10.1126/science.270.5233.53>
- Ehrmann, W. U., & Grobe, H. (1991). Cyclic sedimentation at sites 745 and 746. *Proc., Scientific Results, ODP, Leg 119, Kerguelen Plateau-Prydz Bay*, 119, 225–237.

- Ehrmann, W. U., Grobe, H., & Fütterer, D. K. (1991). Late Miocene to Holocene glacial history of East Antarctica revealed by sediments from sites 745 and 746. *Proc., Scientific Results, ODP, Leg 119, Kerguelen Plateau-Prydz Bay, 119*(1988), 239–260. <https://doi.org/10.2973/odp.proc.sr.119.208.1991>
- Fetterer, F., Knowles, K., Meier, W., Savoie, M., & Windnagel, A. K. (2016). *Updated daily. Sea ice index, version 2*. National Snow and Ice Data Center (NSIDC). <https://doi.org/10.7265/N5736NV7>
- Francois, R., Altabett, M. A., Yu, E. F., Sigman, D. M., Bacon, M. P., Frank, M., et al. (1997). Contribution of Southern Ocean surface-water stratification to low atmospheric CO₂ concentrations during the last glacial period. *Nature*, 389(6654), 929–935. <https://doi.org/10.1038/40073>
- Garcia, H. E., Locarnini, R. A., Boyer, T. P., Antonov, J. I., Baranova, O. K., Zweng, M. M., et al. (2014). In S. Levitus & A. Mishonov Technical (Eds.), *World ocean atlas 2013, volume 4: Dissolved inorganic nutrients (phosphate, nitrate, silicate)* (Vol. 76, p. 25). NOAA Atlas NESDIS.
- Gersonde, R., Crosta, X., Abelmann, A., & Armand, L. (2005). Sea-surface temperature and sea ice distribution of the Southern Ocean at the EPILOG Last Glacial Maximum - A circum-Antarctic view based on siliceous microfossil records. *Quaternary Science Reviews*, 24(7–9), 869–896. <https://doi.org/10.1016/j.quascirev.2004.07.015>
- Hays, J. D., Imbrie, J., & Shackleton, N. J. (1976). Variations in the Earth's Orbit: Pacemaker of the ice ages. *Science*, 194(4270), 1121–1132. <https://doi.org/10.1126/science.194.4270.1121>
- Hillenbrand, C. D., & Cortese, G. (2006). Polar stratification: A critical view from the Southern Ocean. *Palaeogeography, Palaeoclimatology, Palaeoecology*, 242(3–4), 240–252. <https://doi.org/10.1016/j.palaeo.2006.06.001>
- Howell, P. (2012). *ARAND time series and spectral analysis package for the Macintosh*. Brown University.
- Huybers, P. (2006). Early Pleistocene glacial cycles and the integrated summer insolation forcing. *Science*, 313(July), 508–511. <https://doi.org/10.1126/science.1125249>
- Imbrie, J., Boyle, E. A., Clemens, S. C., Duffy, A., Howard, W. R., Kukla, G., et al. (1992). On the structure and origin of major glaciation cycles 1. Linear responses to milankovitch forcing. *Paleoceanography*, 7(6), 701–738. <https://doi.org/10.1029/92PA02253>
- Imbrie, J., Hays, J., Martinson, D., McIntyre, A., Morley, J., Pisias, N., et al. (1984). The orbital theory of Pleistocene climate: Support from a revised chronology of the marine δ¹⁸O record. In A. Berger, J. Imbrie, J. Hays, G. Kukla, & B. Saltzman (Eds.), *Milankovitch and climate, Part 1* (pp. 269–305). D. Reidel Publishing Co.
- Kaiser, E. A., Billups, K., & Bradtmiller, L. (2021). A 1 million year record of biogenic silica in the Indian Ocean sector of the Southern Ocean: Regional versus global forcing of primary productivity. *Paleoceanography and Paleoclimatology*, 36(3). <https://doi.org/10.1029/2020PA004033>
- Kodama, K. P., & Hinnov, L. (2015). *Rock magnetic cyclostratigraphy*. Wiley-Blackwell.
- Kotov, S., & Pálfi, H. (2018). QAnalySeries—A cross-platform time series tuning and analysis tool. In *AGU Fall meeting. Abstracts*.
- Li, F., Ginoux, P., & Ramaswamy, V. (2008). Distribution, transport, and deposition of mineral dust in the Southern Ocean and Antarctica: Contribution of major sources. *Journal of Geophysical Research*, 113(D10), D10207. <https://doi.org/10.1029/2007JD009190>
- Li, M., Hinnov, L., & Lee, K. (2019). Acycle: Time-series analysis software for paleoclimate research and education. *Computers & Geosciences*, 127, 12–22. <https://doi.org/10.1016/j.cageo.2019.02.011>
- Liautaud, P. R., Hodell, D. A., & Huybers, P. J. (2020). Detection of significant climatic precession variability in early Pleistocene glacial cycles. *Earth and Planetary Science Letters*, 536, 116137. <https://doi.org/10.1016/j.epsl.2020.116137>
- Lisiecki, L. E., & Raymo, M. E. (2005). A Pliocene-Pleistocene stack of 57 globally distributed benthic δ¹⁸O records. *Paleoceanography*, 20(1), 1–17. <https://doi.org/10.1029/2004PA001071>
- Matsuoka, K., Skoglund, A., & Roth, G. (2018). *Quantarctica*. Norwegian Polar Institute. <https://doi.org/10.21334/npolar.2018.8516e91>
- Mortlock, R. A., & Froelich, P. N. (1989). A simple method for the rapid determination of biogenic opal in pelagic marine sediments. *Deep-Sea Research, Part A: Oceanographic Research Papers*, 36(9), 1415–1426. [https://doi.org/10.1016/0198-0149\(89\)90092-7](https://doi.org/10.1016/0198-0149(89)90092-7)
- Orsi, A. H., Whitworth, T., & Nowlin, W. D. (1995). On the meridional extent and fronts of the Antarctic Circumpolar Current. *Deep-Sea Research Part I*, 42(5), 641–673. [https://doi.org/10.1016/0967-0637\(95\)00021-W](https://doi.org/10.1016/0967-0637(95)00021-W)
- Raymo, M. E., Lisiecki, L. E., Nisancioglu, K. H., Hemispheres, S., & Instead, O. (2006). Plio-Pleistocene ice volume, Antarctic climate, and the global. *Nature*, 313(July), 492–495. <https://doi.org/10.1126/science.1123296>
- Raymo, M. E., & Nisancioglu, K. (2003). The 41 kyr world: Milankovitch's other unsolved mystery. *Paleoceanography*, 18(1), 1–6. <https://doi.org/10.1029/2002pa000791>
- Ruddiman, W. F., Raymo, M. E., Martinson, D. G., & Backman, J. (1989). Pleistocene evolution: Northern hemisphere ice sheets and North Atlantic Ocean. *Paleoceanography*, 4(4), 353–412. <https://doi.org/10.1029/pa004i004p00353>
- Sakai, H., & Keating, B. (1991). Paleomagnetism of Leg 119 - Holes 737A, 738C, 742A, 745B, and 746A. *Proc., Scientific Results, ODP, Leg 119, Kerguelen Plateau-Prydz Bay, 119*, 751–770. <https://doi.org/10.2973/odp.proc.sr.119.150.1991>
- Shipboard Scientific Party (1989). Site745. In J. Barron, B. Larsen, J. Baldauf, C. Alibert, S. Berkovitz, J.-P. Caulet, et al. (Eds.), *Ocean drilling program* (Vol. 119).
- Starr, A., Hall, I. R., Barker, S., Rackow, T., Zhang, X., Hemming, S. R., et al. (2021). Antarctic icebergs reorganize ocean circulation during Pleistocene glacials. *Nature*, 589(7841), 236–241. <https://doi.org/10.1038/s41586-020-03094-7>
- Sun, Y., Clemens, S. C., An, Z., & Yu, Z. (2006). Astronomical timescale and palaeoclimatic implication of stacked 3.6-Myr monsoon records from the Chinese Loess Plateau. *Quaternary Science Reviews*, 25(1–2), 33–48. <https://doi.org/10.1016/j.quascirev.2005.07.005>
- Tang, Z., Shi, X., Zhang, X., Chen, Z., Chen, M. T., Wang, X., et al. (2016). Deglacial biogenic opal peaks revealing enhanced Southern Ocean upwelling during the last 513 ka. *Quaternary International*, 425, 445–452. <https://doi.org/10.1016/j.quaint.2016.09.020>
- Wu, L., Wang, R., Xiao, W., Ge, S., Chen, Z., & Krijgsman, W. (2017). Productivity-climate coupling recorded in Pleistocene sediments off Prydz Bay (East Antarctica). *Palaeogeography, Palaeoclimatology, Palaeoecology*, 485, 260–270. <https://doi.org/10.1016/j.palaeo.2017.06.018>
- Zhang, Y., Andrade, T., Ravelo, A. C., Gong, L., Holbourn, A., Connock, G., et al. (2023). Aridification of northwest Australia and nutrient decline in the Timor Sea during the 40 kyr world. *Paleoceanography and Paleoclimatology*, 38(10), e2023PA004683. <https://doi.org/10.1029/2023PA004683>